

Measurement of the A_{yy} tensor analyzing power for the ${}^1\text{H}(\vec{d}, pp)n$ reaction in the symmetric constant relative energy geometry

D. A. Low,* E. J. Stephenson, C. Olmer, A. K. Opper,[†] B. K. Park,[‡] P. Schwandt, and S. W. Wissink

Indiana University Cyclotron Facility, 2401 Milo B. Sampson Lane, Bloomington, Indiana 47408

(Received 9 September 1991)

Measurements of the unpolarized triple differential cross section and the A_{yy} tensor analyzing power for the ${}^1\text{H}(d, pp)n$ reaction were made using a 94.5 MeV polarized deuteron beam at the Indiana University Cyclotron Facility. Scattering angles (θ and ϕ) and energy information were recorded for the two emerging protons using large-area wire chambers backed by stopping plastic scintillator detectors. Events were selected that were close to the symmetric constant relative energy geometry in order to enhance the sensitivity of the observables to off-shell and three-body effects. The measurements covered values of α , the center-of-mass angle between the incoming proton and the outgoing neutron, from 72° to 180° . Comparisons are made to Faddeev calculations that use either separable potentials or an exact treatment of the S -wave nucleon-nucleon interaction in conjunction with a perturbative treatment of higher partial waves. While none of these calculations, which use only two-nucleon interactions, is completely satisfactory, there remains too much variation among different theoretical treatments to demonstrate the need for including additional dynamical features in the three-body model.

I. INTRODUCTION

The measurements described in this paper were made to test current models of nuclear reactions that describe three-nucleon systems using the two-body nucleon-nucleon interaction. When three nucleons are present, the kinematic constraints of two-body elastic scattering are relaxed. The nucleon-nucleon interactions can take place off-shell, and experiments with few-body systems test the prescription for off-shell behavior, as well as approximations that facilitate the reaction calculations. In addition, evidence may appear for new dynamical features, such as three-body effects.

The three-nucleon system is the simplest few-body system in which these features might be seen. Since only three particles are involved, observables for this system can in principle be calculated exactly using the Faddeev formalism [1] and the free nucleon-nucleon interaction. This gives us a full theoretical framework within which to test the reaction mechanism or to search for new dynamical effects, without the approximations that are needed in heavier systems to describe the entrance- and exit-channel distorted wave functions or the properties of the bound and scattering states.

In practice, this situation has not yet been realized. Deuteron-proton scattering, the system most easily studied experimentally, introduces a Coulomb interaction which cannot be easily incorporated into the Faddeev calculation. Just to handle the nuclear amplitudes for several partial waves, the calculation must be recast, either with a separable nucleon-nucleon interaction [2] or with a perturbative treatment of the higher angular momenta [3]. Such calculations are becoming more sophisticated, and new, precise measurements including spin dependence could test the current three-body models and

provide a reference point for future theoretical developments. Thus it is useful to identify those reaction channels and observables that are most sensitive to off-shell and three-body effects, the new aspects of the three-body system. It is also important to use sufficiently high bombarding energies so that Coulomb effects and errors in their treatment do not become large enough to compromise any conclusions.

Many measurements have been made for the deuteron-proton and deuteron-neutron elastic scattering channel [4], and existing models provide a satisfactory description of the analyzing powers as well as the cross section at low bombarding energies. As the energy increases the agreement is less satisfactory [5]. Aside from Coulomb effects, the elastic channel is usually dominated by either a single nucleon-nucleon interaction or neutron exchange in which the spectator nucleons undergo only a small momentum change. These processes are well described using nearly on-shell amplitudes and the properties of the deuteron bound state. Therefore elastic scattering, despite its high experimental precision, offers only a limited opportunity to test reaction models or to look for new dynamical effects, and we instead turn our attention to three-body breakup final states.

In order to enhance the sensitivity to off-shell effects, it is helpful to investigate a final state that requires substantial momentum changes for all three nucleons. Likewise, three-body effects become important when the reaction kinematics require the three nucleons to overlap strongly. The collinear geometry, in which one of the nucleons (usually the unobserved neutron) remains at rest in the center-of-mass frame, has been extensively investigated [6], partly because of some early observations that suggested a cross-section enhancement above the values expected from Faddeev calculations. More complete calcu-

lations have brought better agreement and the effect has been largely explained [6]. The symmetric constant relative energy (SCRE) geometry, first suggested by Jain *et al.* [7], offers a geometry that features a strong interference minimum in the cross section as a function of the angles of the outgoing nucleons. It was suggested [7] that this minimum would provide a window where there would be sensitivity to the weaker effects associated with off-shell amplitudes or three-body forces. In this geometry, all three nucleons are emitted in the center-of-mass frame at relative angles of 120° and with equal kinetic energies. The final state can be characterized by the outgoing neutron direction which, in the center-of-mass frame, makes an angle α with respect to the velocity of the incident proton. The protons emerge "symmetrically," which places them in a plane perpendicular to the plane defined by the beam and the emerging neutron.

Measurements of $p + d$ breakup in a SCRE final-state geometry have been reported by van Oers *et al.* for 23-MeV protons [8] and by Bonbright *et al.* for 20- and 39.5-MeV protons [9]. (The latter measurements are at a center-of-mass energy sufficiently close to ours that we are able to compare cross section values.) Several calculations have been made in this geometry, and it is predicted that sensitivities in the interference minimum will increase with rising bombarding energy [10,11]. This has led to a recommendation to pursue cross section and polarization experiments of high precision [12]. A measurement in the SCRE geometry with polarized deuterons had been made earlier at the Indiana University Cyclotron Facility (IUCF) at 79.5 MeV by Schwandt [13]. The Schwandt results had poor statistical precision and limited coverage of the angular distribution due to problems with small solid angles, high singles rates, and radiation damage to the intrinsic germanium detectors used for that experiment. However, calculations made for 80-MeV deuteron energy showed sensitivity for the A_{yy} and A_{xx} tensor analyzing powers to the model and interaction used [13]. It therefore appeared worthwhile to repeat the polarized beam measurements if a scheme could be found that led to greater statistical precision and angle coverage.

We chose to pursue these measurements using large-area wire chambers and plastic scintillation detectors in place of the germanium detectors. The poorer scintillator energy resolution was not a critical factor in discriminating against background, and advantages were obtained from the faster timing characteristics and longer operating life. A large-area system is particularly sensitive to random coincidences, whose rate scales as the product of the two solid angles. By contrast, the breakup coincidence rate scales approximately linearly with the smaller of the two solid angles. To reduce random coincidences, the portion of the active area inside $\theta = 30^\circ$ (where the elastic deuteron flux was large) was shielded against all charged particles. This blocked the two-proton locus for cases where the neutron travelled backward in the center of mass ($\alpha < 72^\circ$). The use of wire chambers to define the scattered proton position allowed considerable flexibility in the analysis, including correction for any geometrical misalignments. Data for all

SCRE points were taken simultaneously with a single fixed setup, thereby minimizing potential problems during the experiment due to adjustments to the equipment.

The experiment is maximally sensitive to the A_{yy} tensor analyzing power when the deuteron spin quantization axis lies in the plane defined by the outgoing neutron and the incident beam direction. Rotations about the beam line that preserved the SCRE kinematics proved to be useful in increasing the statistics of the measurement at the slight expense of sensitivity to A_{yy} . The details of the experiment and the data analysis are presented in Secs. II and III.

For this experiment we chose a beam energy of 94.5 MeV, close to the maximum available from the Indiana University Cyclotron Facility. Raising the energy by 20% relative to the measurements made by Schwandt served both to enhance the detectability of the low energy protons associated with large values of α and to reduce Coulomb effects. However, this also introduces the question of energy dependence in comparison with the older measurement and calculations [13] and increases somewhat the importance of higher partial waves in the three-body calculation. In Sec. IV we present the results of this experiment and compare them with previous results and new calculations. Some data for points not in the SCRE geometry were easily available in the analysis. A comparison of these measurements with calculations is included in Sec. V.

II. EXPERIMENTAL DETAILS

The coordinate system and definitions of the observables follow Ohlsen's conventions [14] as well as the Madison convention [15]. Figure 1 shows the features of the SCRE scattering geometry in the center of mass. All three final-state nucleons emerge with the same kinetic energy. The beam direction defines the \hat{z} axis, and with the outgoing neutron defines the y - z plane. "Symmetry" between the left (L) and right (R) protons requires the

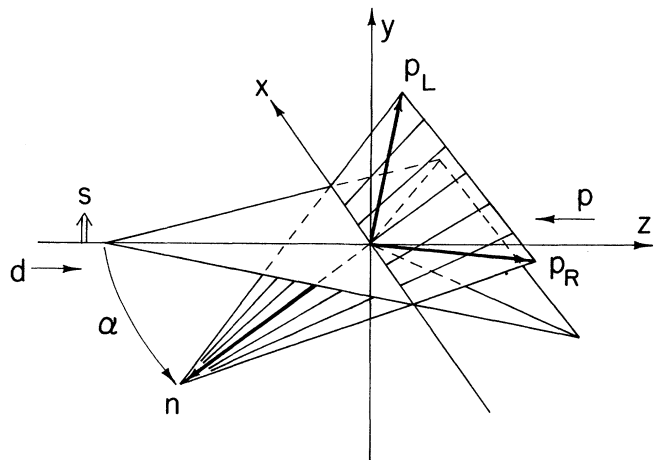


FIG. 1. Sketch showing the $d + p$ coordinate system in the center of mass, the incident deuteron spin quantization axis S , and two triangles whose vertices indicate the directions of the three outgoing nucleons for two values of the angle α .

same angle of elevation from the x - z plane for both particles. The center-of-mass angle between the initial proton velocity and the outgoing neutron velocity is α , the kinematic variable used in this paper. Placing the spin quantization axis of the deuteron beam in the y - z plane and perpendicular to the beam momentum establishes A_{yy} as the variable which describes the sensitivity of the cross section to the tensor polarization of the beam. Because of the left-right symmetry of the final state, parity conservation requires that there be no sensitivity to the vector beam polarization along the same axis, i.e., $A_y = 0$.

Determination of SCRE breakup events in the laboratory system requires detection of the two protons at the same polar angle θ and at complementary azimuthal angles, $\phi_L = 180^\circ - \phi_R$ (with respect to the x axis). Imposition of just these geometric requirements still allows a variety of energy choices for the two protons along a closed locus in $E_L \times E_R$ space, where E_L and E_R are the laboratory energies of the left and right protons, respectively. There are two values along the energy locus where $E_L = E_R$. The SCRE point occurs at the higher summed energy for angles where $\alpha < 135^\circ$ and at the lower other-

wise. With these kinematic requirements on the two protons, definition of SCRE events does not necessitate detecting the neutron.

The polarized deuteron beam was generated in an atomic beam polarized ion source [16]. rf transition units provided tensor polarization of either sign, and a constant negative vector polarization $\frac{1}{3}$ the size of the tensor polarization in magnitude. A nominally unpolarized beam was generated by removing power to all rf transitions. The spin state was changed among these three states every 20 s during data acquisition.

The polarization of the deuteron beam was monitored between the injector and main cyclotrons using a ^3He gas cell and plastic scintillators to detect protons from the $^3\text{He}(d,p)^4\text{He}$ reaction at $\theta_{\text{lab}} = 30^\circ$. The deuterons entered the gas cell with 8.8-MeV energy. The analyzing powers are known from a previous calibration [17] with a normalization error slightly larger than 3%. As the insertion of the gas cell interrupted the beam, measurements of the polarization were made only every 8 to 12 h. All measurements of the beam polarization were statistically consistent with the time-averaged values:

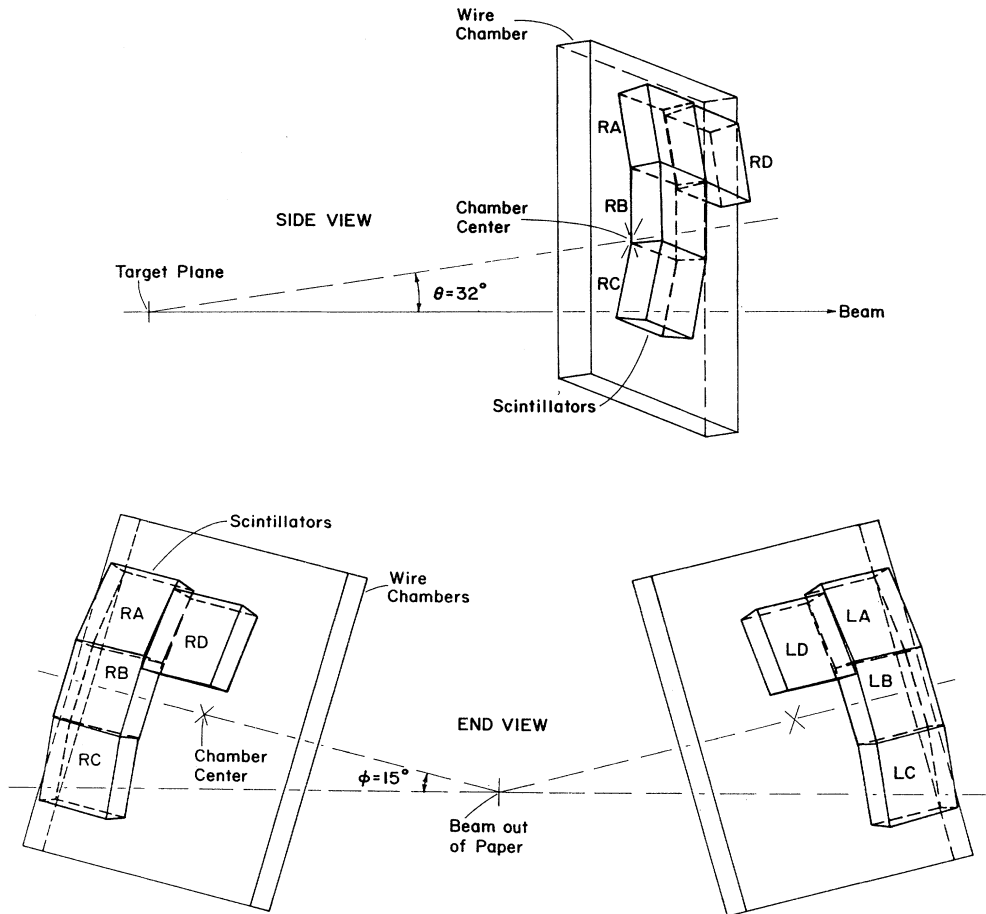


FIG. 2. Two views of the experimental apparatus showing the layout of the wire chambers and plastic scintillators with respect to the target and beam. The letters indicate plastic scintillators ($LA \cdots RD$) on the left (L) and right (R) sides of the beam. The polar angle between the beam direction and the line to the wire chamber center is θ . The azimuthal angle ϕ is measured with respect to the horizontal (x - z) plane.

$p_y = -0.279 \pm 0.008$ and $p_{yy} = 0.827 \pm 0.020$ for the positive tensor state, and $p_y = -0.263 \pm 0.008$ and $p_{yy} = -0.799 \pm 0.019$ for the negative tensor state, where the errors indicate the statistical precision.

The beam energy out of the cyclotron was 94.5 ± 0.1 MeV, as measured by an energy analysis system consisting of two pairs of slits before and after a 45° bending magnet. The energy spread of the beam was less than 100 keV. Beams passing through the experimental apparatus were stopped in a shielded Faraday cup where the number of incident protons was calculated from the integrated charge. The beam current during the measurement was typically 1.2 nA, the value required to keep computer dead times to less than 10%.

The targets were made of polyethylene and mounted on a movable frame. The open area of the frame, 1.9×6.3 cm, was much larger than the beam spot, which was typically 3 mm in diameter. This made it possible to change the illuminated portion of the target often and thus reduce the loss of hydrogen due to target deterioration. The target thickness, as determined by weighing, was typically 5.78 mg/cm². The target chamber incorporated thin Kapton windows through which breakup protons exited the chamber on their way to the wire chamber and scintillator detectors. The space between the Kapton windows and the wire chambers was filled with helium to reduce the effects of energy loss and multiple scattering on the protons.

Figure 2 shows two perspective drawings of the active elements of the detector system. The two wire chambers each contained both x - and y -wire planes. The chambers were filled with a flowing gas mixture of equal parts argon and ethane, bubbled through refrigerated ethanol. The wire spacing was 4 mm, which provided 0.42° resolution on the direction of the breakup proton. Wire chamber signals were read out using a delay line technique in which each wire was separated from its neighbors by a 2-ns delay line. The difference in the arrival times of the signals from each end of the delay line identified the struck wire. Behind each wire chamber were four plastic scintillator detectors with individual phototubes, positioned to span the SCRE locus beyond $\alpha = 72^\circ$. Each had a square entrance face 7.6 cm on a side, and was 5.1 cm deep to stop all breakup protons. The edges of the scintillators were tapered to lie along the direction of the emerging protons. The energy resolution was improved through the addition of a square light guide 2.5 cm deep between the scintillator and the phototube, and the use of gain-stabilized bases. An energy resolution of 2.5% FWHM was obtained for the deuterons elastically scattered from the carbon nuclei in the polyethylene target.

Particle identification in the scintillators was accomplished using the kinematic correlation between the energy deposited in the scintillator and the time of arrival of the particle at the scintillator, measured with respect to an rf signal synchronized to the appearance of a beam pulse at extraction from the cyclotron. Figure 3 shows such a correlation, which easily distinguishes protons from deuterons and tritons, but not from the full range of neutrons from the target. Most neutron events were re-

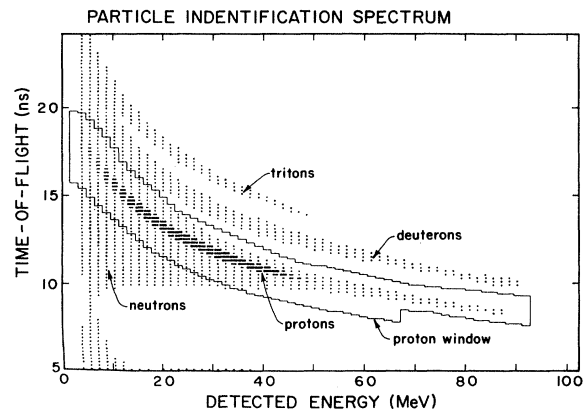


FIG. 3. Two-dimensional particle identification spectrum plotting time of flight as a function of scintillation detector pulse height. The proton, deuteron, and triton loci are shown. The neutron "sea" is indicated, along with the sorting gate for proton events.

jected for lack of a wire chamber signal.

An acceptable event was triggered by the presence of scintillator signals on both sides of the beam within a 30-ns time window. This window was short enough to prevent accidental coincidences from adjacent beam bursts. A small fraction of the single-hit events were also recorded in order to evaluate detector performance by monitoring deuteron elastic scattering from carbon. Events generated by a pulser were used to measure the dead time of the data acquisition electronics. The pulser rate was proportional to the beam intensity on target.

III. DATA ANALYSIS

Considerable freedom was available in the event replay analysis because of the information available from the large-area detector system. This section reviews the analysis procedure and some of the checks made on the quality of the measurements, including the corrections associated with those checks.

The active area of the wire chambers and scintillators was divided into small bins covering a range of $71^\circ \leq \alpha \leq 179^\circ$. These bins were chosen so that $\phi_L = 180^\circ - \phi_R$. To improve the statistics, additional bins were added corresponding to a rotation of the SCRE geometry about the z axis (beam direction) by an angle $\Delta\phi$, i.e., to angles $\phi_L + \Delta\phi$ and $\phi_R + \Delta\phi$, keeping θ fixed. The number of bins for a given value of α ranged from one (at $\alpha = 179^\circ$) to 15 (at $\alpha = 144^\circ$) which covered a range of $\Delta\phi = \pm 15^\circ$. For all angles of α , $\Delta\phi$ was varied symmetrically about zero. When data from all values of $\Delta\phi$ are combined, contributions from analyzing powers that are odd in $\Delta\phi$ will tend to cancel. Analyzing powers, such as A_{xx} , which are even in $\Delta\phi$ will not cancel; estimates using theoretically predicted values for A_{xx} indicate that the contribution to A_{yy} should be less than 0.01. For some of the larger $\Delta\phi$ ranges, it was possible to separate contributions due to A_{xx} experimentally. The results indicated that contributions from A_{xx} to values of A_{yy}

were as small as expected.

Wire chamber position information was extracted by measuring the difference in the time of arrival of the signals from each end of the delay line. For single-hit events, the sum of these times measured relative to the rf signal from the cyclotron should vary only over the range of times required for the ions to drift to the wires within each chamber, which is about 40 ns. Checking this sum provided a way to confirm the quality of each event. Events were occasionally lost due to poor signal quality and the consequent failure of the signal to pass the discriminator threshold at either end of the delay line. Protons identified using scintillator output and time of flight (see Fig. 3) were not adequate to define the efficiency of the chambers, since this selection also contained a substantial neutron flux for which there would be no corresponding wire chamber signal. Instead, the efficiency for each wire chamber was calculated using those coincident events for which the particle detected on the other side was clearly identified as a neutron (low pulse height, correct time, and no wire chamber signal). We assumed that the contribution from $C(p,nn)$ events was negligible compared to the breakup $p(d,pn)$ rate.

An examination of the energy dependence of the wire chamber efficiency showed a constant value of 0.934 ± 0.004 for proton apparent energies above 22 MeV. Below 22 MeV, the efficiency declined. Examination of the proton spectra suggests that this was due to a small contamination from two-neutron coincidences, rather than a real efficiency change. No significant variations (within ± 0.004) were observed with position, side of the beam, or deuteron spin state. This constant efficiency value was used to correct the unpolarized cross sections.

Multiple-hit events, in which at least two scintillators on the same side of the beam recorded a charged particle, constituted less than 0.5% of the total number of events. Because of the resulting ambiguities in the scintillator and wire chamber information, no usable data were available from these events. The contribution of these events to the cross-section calculation was ignored. The fraction of multiple-hit events varied by less than 0.1% among polarization states, and was also ignored in the calculation of the analyzing power.

Despite efforts to reduce the amount of light-insulating paper between adjacent scintillators, some events near the boundaries were lost due to insufficient light collection. The wire intersections which overlaid scintillator gaps were identified, and corrections were generated by averaging rates at adjacent wire intersection points that were fully backed by scintillator material. This correction was assumed to be spin independent, and was included only in the calculation of the unpolarized cross sections.

Two-dimensional plots were made of the pulse heights in the two coincident plastic scintillators. Representative samples for different values of α are shown in Fig. 4. Loci corresponding to the three-body breakup of the deuteron-proton system are clearly evident. There is little background beneath the loci, so background subtraction was not necessary for most values of α . The energy scale for event analysis shown in Fig. 4 was taken from

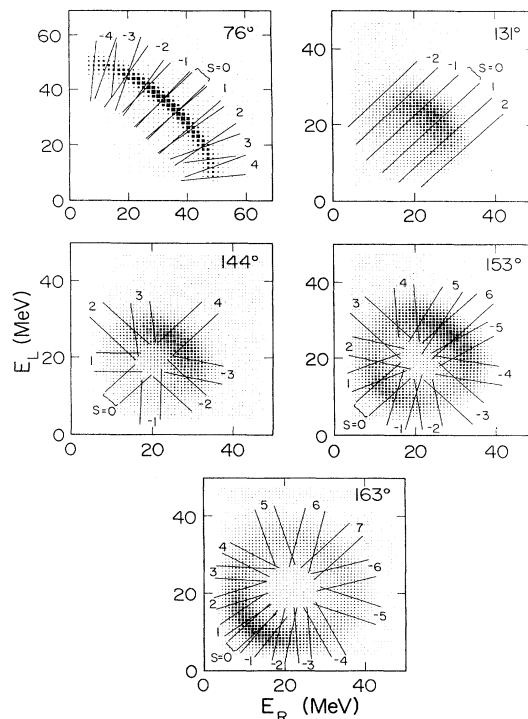


FIG. 4. A selection of two-dimensional pulse-height plots (left versus right) showing the observable portion of the locus for five values of α . Parallel lines indicate sorting gates used for cross section and analyzing power points along the locus.

the pulse height for deuterons elastically scattered from carbon in the polyethylene target. Corrections were made for energy loss in material along the particle path. At the lower proton energies, the loci in Fig. 4 do not correspond to the expectation from three-body kinematics. Subsequent investigation showed this to be due to differences in the response of the plastic scintillator to protons and deuterons [18], and additional energy loss due to material neglected in the original analysis. The symmetry and consistency of the loci indicate that these effects are similar among all eight scintillators, so they do not affect the selection of the SCRE point ($E_L = E_R$). The width of the loci corresponds to the kinematic broadening that originates from the size of the angle bins folded with the intrinsic scintillator energy resolution.

The loci were sliced along parallel straight lines, also shown in Fig. 4, to select areas for calculating cross section and analyzing power. Those labeled $S=0$ correspond to the SCRE geometry. To facilitate calculation of the integrated number of events and to subtract nonlocus background, events within a given area were projected onto an axis parallel to the appropriate pair of straight lines. Sample spectra for the SCRE slices are shown in Fig. 5. In most cases, the various parts of the locus were well isolated from each other, and a simple sum within the indicated limits sufficed to calculate the cross section. The loci for values of α between 122° and 139° were too small to resolve as a ring; the SCRE point was assumed

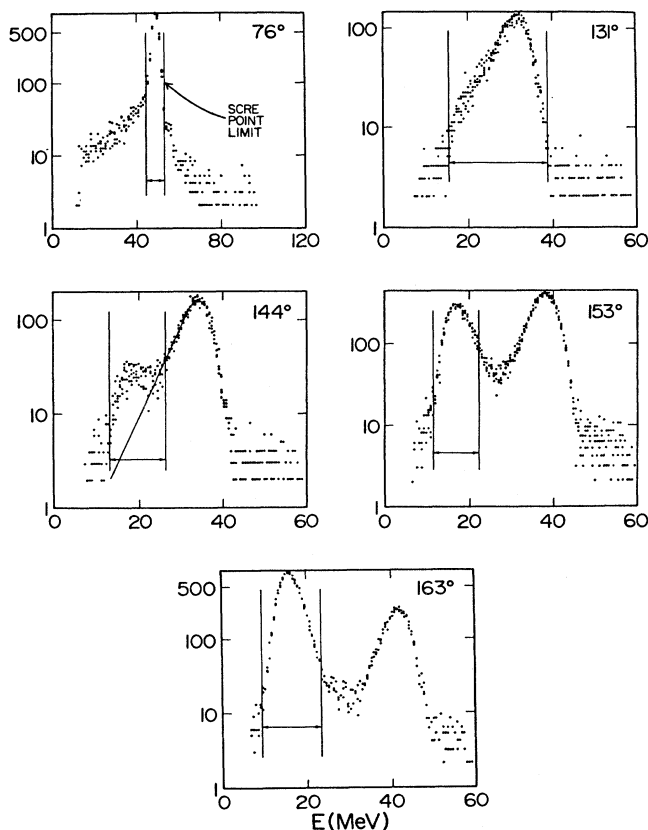


FIG. 5. A selection of one-dimensional projected spectra for the SCRE sorting limits ($S=0$) indicated in Fig. 4. Vertical lines indicate the peak summing limits used for the SCRE data. For $\alpha=144^\circ$, a background subtraction line is shown and the peak sum consists of all the events above the line.

to constitute the entire center section of the locus. Some points near $\alpha=139^\circ$ were omitted from the final data set due to ambiguities in the interpretation. For the midrange of α , where the locus was small, background subtraction was necessary, as indicated for $\alpha=144^\circ$ in Fig. 5. The width of the slice in energy was included in the calculation of the cross section. A correction was made for the errors in the energy scale discussed previously.

Calculations were made for effects in the analysis due to possible angle and position shifts of the beam on target, and a misorientation of the beam quantization axis at the target. For expected values of these misalignment errors, effects on the final results were found to be negligibly small. Comparison of the polarized and unpolarized states gave values for the A_y vector analyzing power that showed no trends with angle (average to -0.003 ± 0.012) and were consistent with zero with a reduced χ^2 of 1.24 (based on statistical errors).

IV. RESULTS AND COMPARISONS WITH THEORETICAL CALCULATIONS

Three classes of calculations were available for comparison with the measurements. The first utilized the

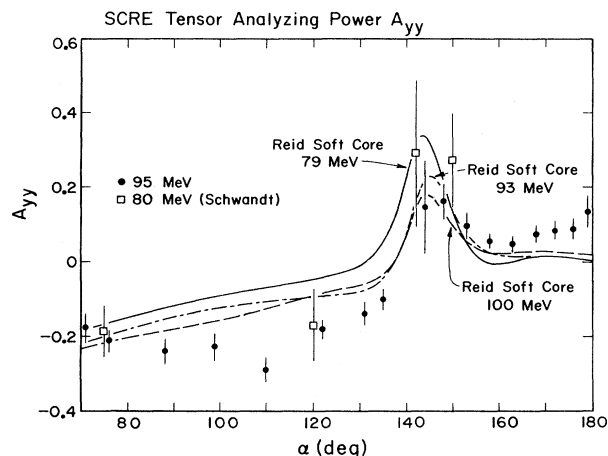


FIG. 6. The A_{yy} tensor analyzing power from this experiment at 94.5 MeV (solid dots) and the 79.5-MeV data of Schwandt (open squares). The curves represent perturbative calculations by Tjon at 79 MeV (solid), 93 MeV (dot-dashed), and 100 MeV (long dashed) using the Reid potential.

program of Doleschall *et al.* and a recent separable potential designed to reproduce nucleon-nucleon phase shifts [19]. Another separable potential was generated by Heidenbauer and Plessas [20] in which greater care was taken with the form of the off-shell amplitudes. This potential was also usable with the Doleschall program. A comparison between these two calculations should provide some indication of the importance of off-shell behavior. These calculations, unfortunately, are lengthy, and are currently available only at the 80-MeV bombarding energy of the original experiment by Schwandt.

A third class of calculations was provided by Tjon [3]. In this case a standard nucleon-nucleon potential (not in separable form) was used to calculate S -wave scattering in the Faddeev formalism. The contribution of higher partial waves was then treated as a perturbation. The Tjon calculations offer the advantage of being easier to execute, and are available for a variety of standard two-

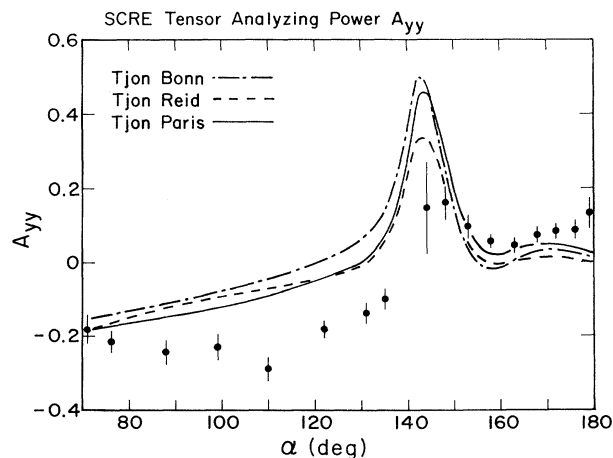


FIG. 7. The A_{yy} tensor analyzing power data at 94.5 MeV compared with three perturbative calculations by Tjon for 80-MeV deuterons using different nucleon-nucleon potentials.

nucleon potentials (Reid [21], Bonn [22], and Paris [23]) and bombarding energies. Thus we can use this set to evaluate the sensitivity of the results to variations in these parameters.

We will discuss the A_{yy} tensor analyzing power results first, and return later to the differential cross section and non-SCRE analyzing power data. We begin with the question of energy dependence, since the new measurements taken at 94.5 MeV may differ systematically from the results and calculations performed near 80 MeV. In Fig. 6, the newly measured A_{yy} values are shown together with data from Schwandt. The 79.5-MeV A_{yy} measurements agree within their experimental errors with the values from the present experiment. Figure 6 also contains calculations at three deuteron bombarding energies made using the Tjon program and the Reid nucleon-nucleon potential. The energy dependence is small, and seems irregular between 93 and 100 MeV. Nevertheless, these calculations suggest that for comparison with the new measurements the theoretical results at 80 MeV should be shifted negatively by amounts between 0.03 and 0.06 for values of $\alpha < 150^\circ$. Larger shifts near $\alpha = 145^\circ$ may only reflect changes in the position of the interference peak.

A comparison of calculations based on potential models from different groups provides a way to estimate the uncertainty introduced by the choice of any particular model to represent the nucleon-nucleon scattering data. Figure 7 shows the present measurements of the tensor analyzing power compared with three calculations from Tjon using the potentials from Reid, Bonn, and Paris, all at 80 MeV. Variations of about 0.05 are typically seen among the various potential models.

Finally, an assessment of the need for additional dynamical information in order to understand three-body systems is desirable. The best available means of addressing this issue is shown in Fig. 8, which displays the three classes of calculation. We chose the calculation of Tjon based on the Paris potential to represent this class. For ease of comparison, all of the calculations were made at 80 MeV.

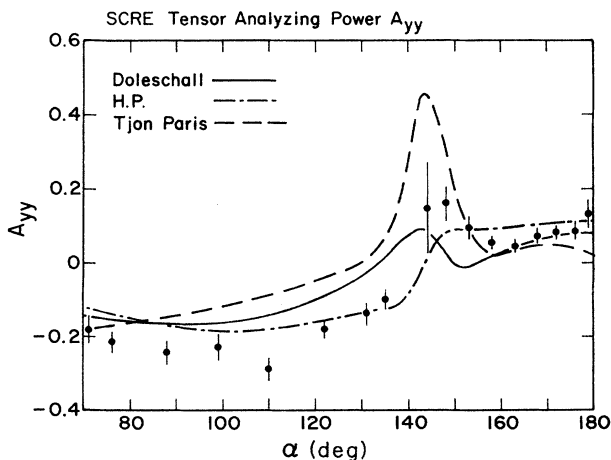


FIG. 8. The A_{yy} tensor analyzing power data at 94.5 MeV compared with three classes of calculations for 80-MeV deuteron energy.

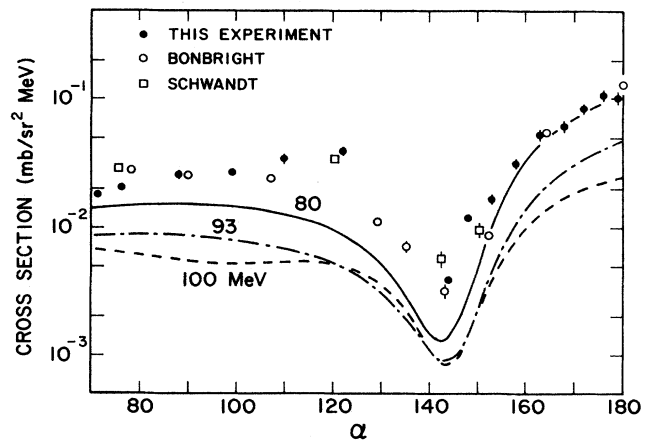


FIG. 9. Measurements of the triple differential cross section $d^3\sigma/dE_{23}d\Omega_{23}d\Omega_{1-23}$ in Jacobi coordinates for the present experiment at 94.5 MeV (solid dots) and the previous experiments of Bonbright (open circles) and Schwandt (open squares). The curves represent perturbative calculations by Tjon at three deuteron bombarding energies.

All of the calculations shown in Fig. 8 reproduce some qualitative features of the data, but all differ significantly from the data over some range of angles. Closest to the data is the calculation using the Heidenbauer and Plessas potential. Almost all of the measurements lie within a band about this calculation of a width suggested by our estimate of the potential model uncertainty. Agreement for this case would be even better at $\alpha < 120^\circ$ if the energy dependence moved the calculation to more negative values in accord with the trend shown in Fig. 6. This calculation also differs from the one using the potential of Doleschall, indicating the importance of the treatment of the off-shell potential.

Both of the separable-potential calculations differ substantially from those by Tjon, which may indicate a problem with either the separable potentials used with the Doleschall program or the perturbative scheme employed

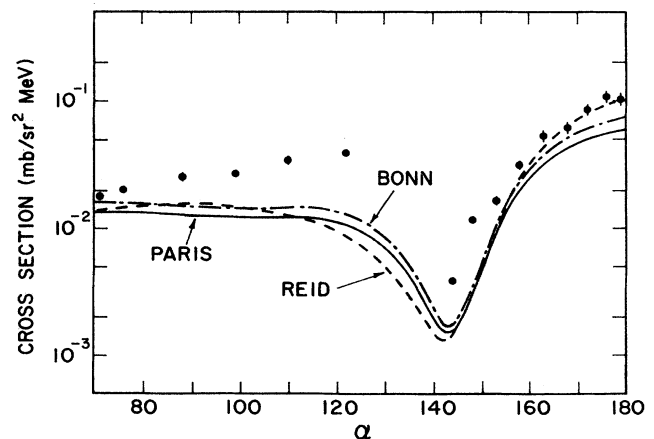


FIG. 10. Measurements of the triple differential cross section at 94.5 MeV compared with three perturbative calculations by Tjon at 80 MeV using different nucleon-nucleon potentials.

by Tjon. The perturbative scheme does produce a larger positive excursion near $\alpha = 150^\circ$, but otherwise is less adequate to describe the trend of the measurements.

While it is tempting to conclude that the better off-shell treatment used in the Heidenbauer-Plessas calculation is advantageous, the variations among the calculations leave some question concerning whether there might be other difficulties present. Thus it is premature to conclude that there are systematic differences large enough to suggest the presence of other dynamical features, such as three-body forces.

A similar set of comparisons is available for the triple differential cross section. To facilitate comparisons with calculations and the Bonbright measurements, all laboratory values have been transformed to $d^3\sigma/dE'_{23}d\Omega'_{23}d\Omega'_{1-23}$ in relative Jacobi coordinates using the equations in the Appendix. We will follow the same development used to discuss the analyzing power measurements, and begin with the issue of energy dependence. The measurements of the present experiment are shown in Fig. 9 together with the values from Bonbright and Schwandt. Despite being at nearly the same energy, the measurements of Schwandt are larger than those of Bonbright for α between $\sim 120^\circ$ and 150° . This complicates the question as to what the experimental energy dependence is. Aside from these discrepancies, the cross section appears to be relatively constant with bombarding energy. Also shown in Fig. 9 is the energy-dependent trend predicted by the Tjon calculations using the Reid soft-core potential. The downward trend with increasing energy in the Tjon result is in contrast to the measurements, especially near $\alpha = 180^\circ$ where there is a factor of 2 reduction predicted for every 10-MeV increase in energy.

Compared to the differences between measurements and calculations (all near 80 MeV), the differences shown in Fig. 10 among the three potential models are not particularly large. The Bonn and Paris calculations are, in fact, very similar in shape and seem to differ only slightly in normalization.

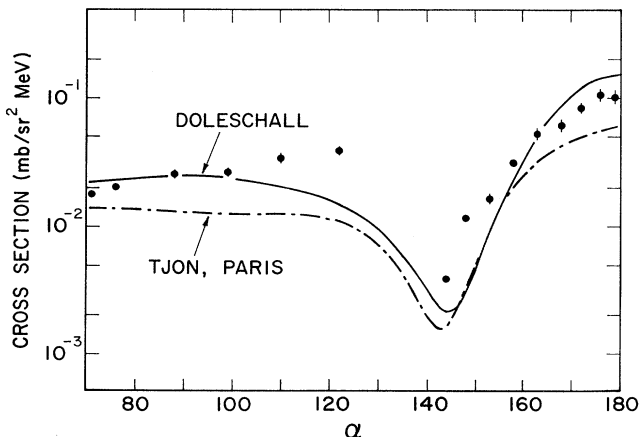


FIG. 11. Measurements of the triple differential cross section at 94.5 MeV compared with two classes of calculations at 80 MeV.

Only the cross sections from the Doleschall potential were available, and they are compared with the Tjon-Paris calculation and the data in Fig. 11. The separable potential gives generally larger cross section values that come close to the data at either end of the measured angular distribution. Again, the differences between these calculations are large, and preclude any meaningful comparisons among the potential models. Unlike the analyzing power, the energy dependence is not well described and needs further attention.

V. NON-SCRE RESULTS AND CALCULATIONS

Other points on the two-dimensional loci shown in Fig. 4 can be analyzed for differential cross section and analyzing power information. On an energy scale moving along the locus from the SCRE point to the point opposite, values of the A_{yy} tensor analyzing power are shown in Fig. 12. (The length of the energy scale has been normalized so that a complete circuit along the locus spans from -1 to 1 .) The variations are symmetric about 0, as required by the geometrical constraints of the experiment. There also appears to be a smooth variation from the tensor analyzing power values from the SCRE point to the non-SCRE equal-energy point. Thus any new information is most clearly seen at the non-SCRE equal-energy point. The tensor analyzing power for this point is shown in Fig. 13. For convenience, α is used as the kinematic variable even though these points do not satisfy the requirements for the SCRE geometry and α is no longer the angle between the incoming proton and the outgoing neutron.

Calculations from Tjon are available for the non-SCRE equal-energy point. Shown in Fig. 13 are two calculations with different potentials. As in the case of the

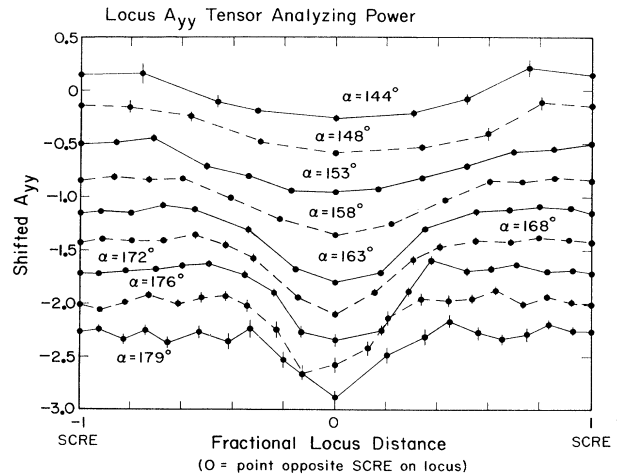


FIG. 12. Measurements of the A_{yy} tensor analyzing power for several values of α (defined only at the SCRE point) plotted as a function of fractional position along the kinematic locus (see Fig. 4). The horizontal axis includes the entire locus with the same SCRE point values plotted at both -1 and 1 . The tensor analyzing powers are shifted by -0.3 for each successive value of α beyond 144° , and the lines are guides for the eye.

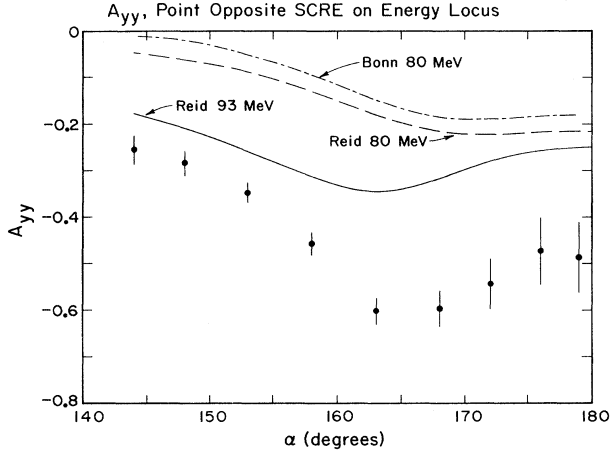


FIG. 13. The A_{yy} tensor analyzing power for the non-SCRE equal-energy point on the kinematic locus (see Fig. 4). The curves represent perturbative calculations by Tjon for two potentials and two energies. The kinematic variable α does not apply and is used here for convenience only.

SCRE data, the difference is small. In this case, however, a large change is seen with bombarding energy, since the Reid calculation at 93 MeV differs substantially from the same calculation at 80 MeV. None of the calculations are particularly close to the measurements. Lacking calculations using other techniques, it is difficult to know whether this large difference is again an issue raised by the approximation in the calculation or an indication of some deficiency in the three-body model.

VI. CONCLUSIONS

We have measured the triple differential cross section and the A_{yy} tensor analyzing power for deuteron breakup on the proton in the SCRE geometry. This final-state geometry is expected to be particularly sensitive to the off-shell treatment of the nucleon-nucleon interaction and the presence of three-body effects.

A number of calculations were compared with the measurements, some using separable potentials and others using a perturbative approach to solve the Faddeev equations. At the SCRE point, variations in the tensor analyzing power with energy and nucleon-nucleon potential were smaller than the differences among the different types of calculation. The best reproduction of the tensor analyzing power was achieved with the separable potential of Heidenbauer and Plessas incorporated into the Doleschall program. In comparison with the cross section, the Doleschall separable potential gave the largest values and hence the best agreement with the measurements, but the predictions of the Heidenbauer and Plessas potentials were not available for comparison. The variations among the different types of calculation make it difficult to assess their reliability and whether there is any need for additional dynamical features in the three-body model. The quality of the measurements is good and experimental errors are generally small. Except for

inconsistencies in the 80-MeV cross-section values, the errors are smaller than the variations among the models. Thus we hope that these new data will be beneficial for the evaluation of future three-body calculations in this system.

ACKNOWLEDGMENTS

This work was supported in part by the National Science Foundation. The authors would like to thank R. E. Brown and J. A. Tjon for assistance with the calculations shown in this paper.

APPENDIX: TRANSFORMATION BETWEEN LABORATORY AND CENTER-OF-MASS OR JACOBI FRAMES IN THE SCRE GEOMETRY

For comparison among experiments with different entrance channels (proton or deuteron beam), it is expedient to reduce all observables to a common system. In this Appendix we will denote laboratory quantities without a prime, and their equivalents in another frame with a prime. Projectile and target variables in the entrance channel will be denoted by p and t , respectively. In the three-body exit channel, particles 1 and 2 are observed, and particle 3 is not. The angle α is defined as the angle between the incident proton momentum and the momentum of outgoing particle 3 in the center-of-mass frame. For simplicity we will assume $m_1 = m_2 = m_3 = m$ and use nonrelativistic kinematics.

The triple differential cross section in the center-of-mass and laboratory frames is related by the Jacobian J :

$$\frac{d^3\sigma}{dE'_1 d\Omega'_1 d\Omega'_2} = J \frac{d^3\sigma}{dE_1 d\Omega_1 d\Omega_2}, \quad (\text{A1})$$

where Ω_i is the detector solid angle for particle i . Since we used α , the center-of-mass angle between the incident proton and outgoing neutron, as the kinematic variable, we will express the Jacobian in terms of α .

In the SCRE geometry

$$E'_1 = E'_2 = E', \quad E_1 = E_2 = E, \quad (\text{A2})$$

and

$$\theta'_1 = \theta'_2 = \theta', \quad \theta_1 = \theta_2 = \theta, \quad (\text{A3})$$

where the angles are referenced to a z axis along the beam direction. In this case

$$J = \frac{E'}{E} \frac{\partial\theta}{\partial\theta'}. \quad (\text{A4})$$

In the center of mass, E' is the energy available for each nucleon

$$E' = \frac{1}{3} \left[\frac{E_p m_t}{m_p + m_t} + Q \right], \quad (\text{A5})$$

where Q is the reaction Q value. The laboratory energy E is obtained by transforming to a frame traveling in the beam direction with a beam velocity V . Then

$$E = E' + a\sqrt{E'}\cos\alpha + a^2, \quad (\text{A6})$$

$$a^2 = \frac{mV^2}{2} = \frac{mm_p E_p}{(m_p + m_t)^2} . \quad (\text{A7})$$

The relation to the frame moving with velocity V also gives the relationship between angles:

$$\sqrt{E'} \sin \theta' = \sqrt{E} \sin \theta , \quad (\text{A8})$$

$$\sqrt{E'} \cos \theta' + a = \sqrt{E} \cos \theta . \quad (\text{A9})$$

From geometry

$$\cos \theta' = \frac{1}{2} \cos \alpha \quad (\text{A10})$$

and the azimuthal angle of the detected particle relative to the horizontal plane is the same in both frames

$$\tan \phi = \tan \phi' = \frac{1}{\sqrt{3}} \sin \alpha . \quad (\text{A11})$$

Considering the dependence of E and θ on θ' , the remaining factor in the Jacobian of Eq. (A4) can now be written as

$$\frac{\partial \theta}{\partial \theta'} = 1 - \frac{a \cos \theta}{\sqrt{E}} . \quad (\text{A12})$$

In the center-of-mass system, the center-of-mass point is the common origin for all radius vectors. In relative Jacobi coordinates, used in most Faddeev calculations, different radius vectors are used to specify the particle separations. Particles 2 and 3 (the latter not observed) are referred to

$$\mathbf{r}_{23} = \mathbf{r}_2 - \mathbf{r}_3 \quad (\text{A13})$$

and particle 1 is referred to the center of mass of particles 2 and 3

$$\mathbf{r}_{1-23} = \mathbf{r}_1 - \frac{1}{2}(\mathbf{r}_2 + \mathbf{r}_3) . \quad (\text{A14})$$

Likewise the relative momenta are defined by

$$\mathbf{p}_{23} = \frac{1}{2}(\mathbf{p}_2 - \mathbf{p}_3) , \quad (\text{A15})$$

$$\mathbf{p}_{1-23} = \frac{2}{3}[\mathbf{p}_1 - \frac{1}{2}(\mathbf{p}_2 + \mathbf{p}_3)] . \quad (\text{A16})$$

In the laboratory frame the incident momentum is connected to these momenta through

$$\mathbf{p}_{\text{in}} = \mathbf{p}_1 + \mathbf{p}_2 + \mathbf{p}_3 . \quad (\text{A17})$$

In the SCRE geometry

$$|\mathbf{p}_1| = |\mathbf{p}_2| = p . \quad (\text{A18})$$

The Jacobian for the transformation from the laboratory frame to this frame is

$$\frac{d^3 \sigma}{dE'_{23} d\Omega'_{23} d\Omega'_{1-23}} = J \frac{d^3 \sigma}{dE_1 d\Omega_1 d\Omega_2} \quad (\text{A19})$$

and is given by

$$J = \frac{1}{2} \frac{p_{1-23}}{p} \frac{p_{23}}{p} \left[1 - \frac{1}{3} \frac{p_{\text{in}}}{p} \cos \theta \right] , \quad (\text{A20})$$

where

$$\left[\frac{p_{1-23}}{p} \right]^2 = 1 + \frac{1}{9} \left[\frac{p_{\text{in}}}{p} \right]^2 - \frac{2}{3} \left[\frac{p_{\text{in}}}{p} \right] \cos \theta , \quad (\text{A21})$$

$$\left[\frac{p_{23}}{p} \right]^2 = \frac{5}{4} + \frac{1}{4} \left[\frac{p_{\text{in}}}{p} \right]^2 - \frac{3}{2} \left[\frac{p_{\text{in}}}{p} \right] \cos \theta + \cos \theta_{12} , \quad (\text{A22})$$

$$\left[\frac{p_{\text{in}}}{p} \right] = \frac{m_p E_p}{mE} , \quad (\text{A23})$$

and

$$\cos \theta_{12} = 1 - 2 \sin^2 \theta \cos^2 \phi . \quad (\text{A24})$$

*Present address: Mallinckrodt Institute of Radiology, Department of Radiation Oncology, 510 S. Kingshighway, St. Louis, MO 63110.

†Present address: University of Alberta Nuclear Research Centre, Edmonton, Alberta, Canada T6G 2N5.

- [1] L. D. Faddeev, Zh. Eksp. Teor. Fiz. **39**, 1459 (1961) [Sov. Phys. JETP **12**, 1014 (1961)].
- [2] P. Doleschall, Nucl. Phys. **A201**, 264 (1973); see also E. O. Alt, P. Grassberger, and W. Sandhas, Nucl. Phys. **B2**, 167 (1967).
- [3] C. Stolk and J. A. Tjon, Nucl. Phys. **A295**, 384 (1978).
- [4] For a review, see R. A. Brandenburg, in *The Three-Body Force in the Three-Nucleon System*, edited by B. L. Berman and B. F. Gibson (Springer-Verlag, New York, 1986), p. 186; also experiments, such as, C. R. Howell, W. Tornow, K. Murphy, H. G. Pfützner, M. L. Roberts, Anli Li, P. D. Felsher, R. L. Walters, I. Šlaus, P. A. Treado, and Y. Koike, Few-Body Systems **2**, 19 (1987).
- [5] J. Arvieux, A. Boudard, G. Gaillard, Nguyen van Sen, G. Perrin, Ye Yanlin, and Y. Koike, Few-Body Systems **3**, 27 (1987).

- [6] F. D. Correll, R. E. Brown, G. G. Ohlsen, R. A. Hardkopf, N. Jarmie, J. M. Lambert, P. A. Treado, I. Šlaus, P. Schwandt, and P. Doleschall, Nucl. Phys. **A475**, 407 (1987), and references therein.
- [7] M. Jain, J. G. Rogers, and D. P. Saylor, Phys. Rev. Lett. **31**, 838 (1973).
- [8] W. T. H. van Oers, in *Proceedings of the Seventh International Conference on Few Body Problems in Nuclear and Particle Physics*, edited by A. N. Mitra *et al.* (North-Holland, Amsterdam, 1976), p. 746.
- [9] D. I. Bonbright, A. M. MacDonald, W. T. H. van Oers, J. W. Watson, H. S. Caplan, J. M. Cameron, J. G. Rogers, J. Soukup, W. M. Kloet, C. Stolk, and J. A. Tjon, Phys. Rev. **C20**, 879 (1979).
- [10] H. O. Klages, in *The Three-Body Force in the Three-Nucleon System* (Ref. [4]), p. 203.
- [11] J. H. Stuivenberg and R. van Wageningen, Nucl. Phys. **A304**, 141 (1978).
- [12] E. L. Tomusiak and H. R. Weller, in *The Three-Body Force in the Three-Nucleon System* (Ref. [4]), p. 177.
- [13] P. Schwandt, W. W. Jacobs, H. O. Meyer, E. J. Stephen-

- son, J. Q. Yang, R. E. Brown, N. Jarmie, P. Doleschall, and W. T. H. van Oers, Indiana University Cyclotron Facility Scientific and Technical Report, 1983, p. 61; and reviewed in J. Arvieux and J. M. Cameron, *Adv. Nucl. Phys.* **18**, 107 (1987).
- [14] G. G. Ohlsen, *Nucl. Instrum. Methods* **179**, 283 (1981).
- [15] The Madison Convention, in *Proceedings of the Third International Symposium on Polarization Phenomena in Nuclear Reactions*, edited by H. H. Barschall and W. Haeberli (University of Wisconsin Press, Madison, 1971), p. xxv.
- [16] W. Haeberli, *Annu. Rev. Nucl. Sci.* **17**, 373 (1967).
- [17] D. A. Low, A. D. Bacher, J. D. Brown, M. S. Cantrell, V. R. Cupps, D. L. Friesel, J. Gering, W. P. Jones, C. Olmer, P. Schwandt, and E. J. Stephenson, Indiana University Cyclotron Facility Scientific and Technical Report, 1983, p. 156.
- [18] W. K. Pitts, Ph.D. thesis, University of Indiana, 1987; based on measurements reported in R. L. Craun and D. L. Smith, *Nucl. Instrum. Methods* **80**, 239 (1970).
- [19] P. Doleschall, W. Gruebler, V. König, P. Schmelzbach, F. Sperisen, and B. Jenny, *Nucl. Phys. A* **380**, 72 (1982).
- [20] J. Haidenbauer and W. Plessas, *Phys. Rev. C* **30**, 1822 (1984); based on D. Ernst, C. M. Shakin, and R. M. Thaler, *ibid.* **8**, 507 (1973).
- [21] Roderick V. Reid, Jr., *Ann. Phys. (N.Y.)* **50**, 411 (1968).
- [22] R. Machleidt, *Adv. Nucl. Phys.* **19**, 189 (1989).
- [23] M. Lacombe, B. Loiseau, J. M. Richard, R. Vinh Mau, J. Côte, P. Pires, and R. de Tournel, *Phys. Rev. C* **21**, 861 (1980).